

Scalable synthesis of hierarchically structured carbon nanotube-graphene fibres for capacitive energy storage

Dingshan Yu¹, Kunli Goh¹, Hong Wang¹, Li Wei¹, Wenchao Jiang¹, Qiang Zhang², Liming Dai^{3*} and Yuan Chen^{1*}

Micro-supercapacitors are promising energy storage devices that can complement or even replace batteries in miniaturized portable electronics and microelectromechanical systems. Their main limitation, however, is the low volumetric energy density when compared with batteries. Here, we describe a hierarchically structured carbon microfibre made of an interconnected network of aligned single-walled carbon nanotubes with interposed nitrogen-doped reduced graphene oxide sheets. The nanomaterials form mesoporous structures of large specific surface area ($396 \text{ m}^2 \text{ g}^{-1}$) and high electrical conductivity (102 S cm^{-1}). We develop a scalable method to continuously produce the fibres using a silica capillary column functioning as a hydrothermal microreactor. The resultant fibres show a specific volumetric capacity as high as 305 F cm^{-3} in sulphuric acid (measured at 73.5 mA cm^{-3} in a three-electrode cell) or 300 F cm^{-3} in polyvinyl alcohol (PVA)/ H_3PO_4 electrolyte (measured at 26.7 mA cm^{-3} in a two-electrode cell). A full micro-supercapacitor with PVA/ H_3PO_4 gel electrolyte, free from binder, current collector and separator, has a volumetric energy density of $\sim 6.3 \text{ mWh cm}^{-3}$ (a value comparable to that of 4 V-500 μAh thin-film lithium batteries) while maintaining a power density more than two orders of magnitude higher than that of batteries, as well as a long cycle life. To demonstrate that our fibre-based, all-solid-state micro-supercapacitors can be easily integrated into miniaturized flexible devices, we use them to power an ultraviolet photodetector and a light-emitting diode.

The continued miniaturization of portable electronics requires energy storage devices with large volumetric energy densities^{1–4}.

Although suffering from sluggish charge/discharge processes and limited cycle life, microbatteries currently remain the device of choice for this type of application⁵. Micro-supercapacitors (micro-SCs)^{5,6} are promising alternatives as they can provide higher power densities, faster charge/discharge rates and much longer lifetimes^{2,5}. However, the key challenge for their use in practical applications is increasing their energy density to values close to and even exceeding those of microbatteries without compromising other electrochemical characteristics^{1,2,6}. To this end, electrodes with large volumetric capacitance need to be developed. Materials with high electrical conductivity and accessible surface area can achieve high electrical double layer (EDL) capacitances, which can then be further enhanced by means of the pseudocapacitance associated with surface functional groups and/or pseudocapacitive components^{7,8}. Although various thin-film micro-SCs based on transition metal oxides⁹ and conducting polymers^{10,11} have recently been fabricated using printing, lithography and laser writing^{1–3}, these devices often suffer from short cycle lives, low stability and poor rate capability. In an alternative approach, micro-SCs based on carbon nanomaterials, including carbon onion¹, reduced graphene oxide (rGO)³, carbide-derived carbon⁵, graphene dots¹² and carbon nanotube (CNT)/rGO composites¹³, have exhibited excellent rate capabilities and stability, but low volumetric energy density. Recently, fibre-shaped micro-SCs have been developed for flexible and wearable electronics^{4,14}, based on carbon fibres¹⁵, CNT fibres^{16,17}, rGO fibres¹⁸ and even carbon-based composite fibres

containing pseudo-capacitive materials^{19–22}. In all cases, however, it remains challenging to increase the volumetric energy density of micro-SCs without sacrificing device power density and cycle life.

A general strategy to increase volumetric energy density is to develop porous conductive electrode materials with sufficiently high packing density to maximize the utilization of the limited volume of a micro-SC. In this context, graphene sheets are widely regarded as a promising electrode material because they have ultrahigh surface area and excellent conductivity as well as high mechanical and chemical stability⁶. Graphene can be assembled into various interesting structures, including one-dimensional fibres¹⁸, two-dimensional films⁶ and three-dimensional foams²³, which can demonstrate high gravimetric capacitances but poor volumetric performances. A possible explanation of this behaviour lies in the strong intersheet π - π interaction, which, while increasing the packing density, does not allow high ion accessibility. To reduce stacking, graphene–CNT composites have been proposed and fabricated. In particular, two-dimensional CNT/rGO hybrid films^{24,25} and three-dimensional vertically aligned CNT/graphene pillars^{26–28} have shown significantly improved electrochemical performances. For practical applications, however, their volumetric energy densities would still need to be improved significantly^{26–28}.

Here, we describe the scalable synthesis of a hierarchically structured carbon microfibre made of a single-walled carbon nanotube (SWNT)/nitrogen-doped rGO sheet interconnected network architecture that shows excellent electrical conductivity and high packing density while maintaining a large ion-accessible surface

¹School of Chemical and Biomedical Engineering, Nanyang Technological University, 62 Nanyang Drive, Singapore 637459, Singapore, ²Beijing Key Laboratory of Green Chemical Reaction Engineering and Technology, Department of Chemical Engineering, Tsinghua University, 1 Tsinghua Road, Beijing 100084, China, ³Center of Advanced Science and Engineering for Carbon (Case4Carbon), Department of Macromolecular Science and Engineering, Case Western Reserve University, Cleveland, Ohio 44106, USA. *e-mail: chenyuan@ntu.edu.sg; liming.dai@case.edu

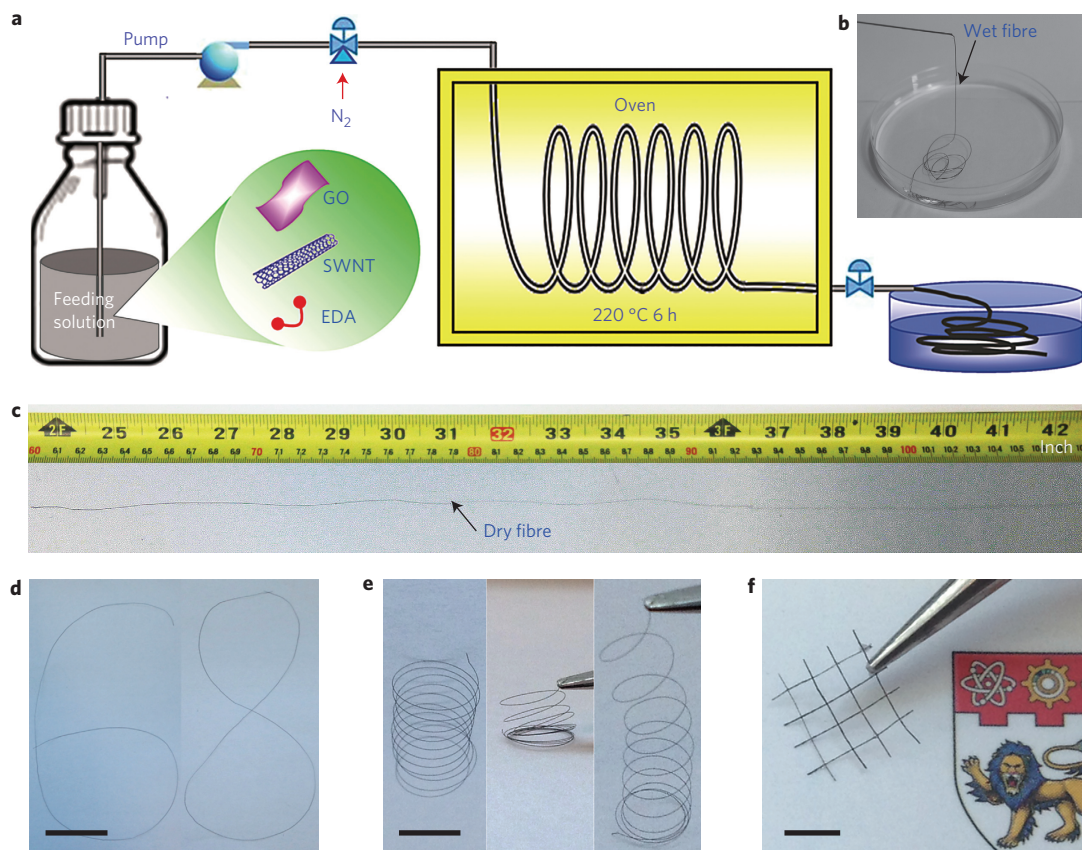


Figure 1 | Schematic of the synthesis of carbon hybrid microfibres. **a**, The fibre was synthesized by injecting a homogeneous solution containing acid-oxidized SWNTs, GO and EDA through a pump into a flexible silica capillary column, followed by *in situ* thermal treatment in an oven at 220 °C for 6 h before a continuous fibre was pushed into a water reservoir by a pressurized nitrogen flow. **b**, Photograph of the as-prepared fibres collected in water. **c**, A dry fibre with diameter of ~50 μm and length of ~0.5 m (~20 inches). **d**, Planar structures obtained by bending fibres. **e**, Compressed and stretched fibre springs. **f**, A knitted textile fabricated from fibres. All scale bars, 0.5 cm.

area. Micro-SCs fabricated with these fibres show volumetric energy densities comparable to those of thin-film lithium batteries, without compromising cyclability and rate capability.

Synthesis of carbon hybrid microfibres

Hydrothermal processes are widely used to synthesize materials in high-temperature aqueous solutions at high vapour pressures using pressure vessels called autoclaves. Fused silica capillary columns are generally used for chromatographic separation, which, unlike fragile glass tubes¹⁸, are flexible and have good high-temperature and pressure tolerance. We employed a fused-silica capillary column as a hydrothermal microreactor for the scalable production of SWNT/rGO fibres, as shown in Fig. 1a. Nitric-acid-treated SWNTs and GO (Supplementary Fig. 1) were combined to form hybrid microfibres in the presence of ethylenediamine (EDA) as the nitrogen dopant to dope GO with concomitant reduction during the hydrothermal process²⁹. By so doing, we took advantage of the following synergistic effects. First, GO is a good surfactant with which to disperse SWNTs, while SWNTs hinder the restacking of GO³⁰, resulting in a homogeneous aqueous suspension. Second, heteroatom doping not only improves surface conductivity and wettability, but also induces pseudocapacitance in carbon nanomaterials^{31,32}. More importantly, EDA, with its two $-\text{NH}_2$ end groups, can act as a molecular ‘end-anchoring’ reagent to bind acid-oxidized SWNTs and GO to create the three-dimensional pillared vertically aligned SWNT/rGO architectures²⁷ via self-assembling within the fibre confinement³³, which is oriented along the fibre length (Fig. 2g–i) by the shear force while flowing through the silica capillary column. Within the SWNT/rGO

assemblies, the aligned SWNTs, which have a relatively low EDL capacitance, have excellent electrical conductivity and provide an outstanding rate capability³⁴, while the large-surface-area rGO offers a high EDL capacitance (theoretically, 550 F g^{-1})⁶. These synergistic effects are responsible for the enhanced electrochemical performances observed from our hybrid fibres.

Owing to the small size and mechanical flexibility of the silica capillary columns, multiple long columns can be integrated with a valve switching system for continuous fibre production. As a proof-of-concept study, two 5-m-long capillary columns were used to produce 50-m-long fibres in 48 h, suggesting a production yield of 1 m h^{-1} (Supplementary Fig. 2). The production rate was tunable by adjusting the synthesis conditions.

To identify the optimum composition of the hybrid fibres for micro-SC applications, several fibres with different SWNT/GO mass ratios of 0:1, 1:8, 1:4 and 1:1 (denoted rGO fibre, fibre-1, fibre-2 and fibre-3, respectively) were produced. The continuous fibres could not form when the mass fraction of GO was below 50 wt% (Supplementary Fig. 3). The as-synthesized wet fibres (260–300 μm in diameter) were dried in air for 4 h, resulting in a five- to sixfold shrinkage in diameter to 40–60 μm due to the capillary force during water evaporation (Table 1)³⁵.

Structural characterization of carbon hybrid microfibres

The as-prepared dry hybrid fibres exhibited good tensile strength (84–165 MPa, Supplementary Fig. 4), comparable to those of wet-spun rGO and SWNT fibres^{36,37}. They were also flexible, and could be bent into different shapes or woven into textile structures (Fig. 1d–f). The high packing density and large ion-accessible

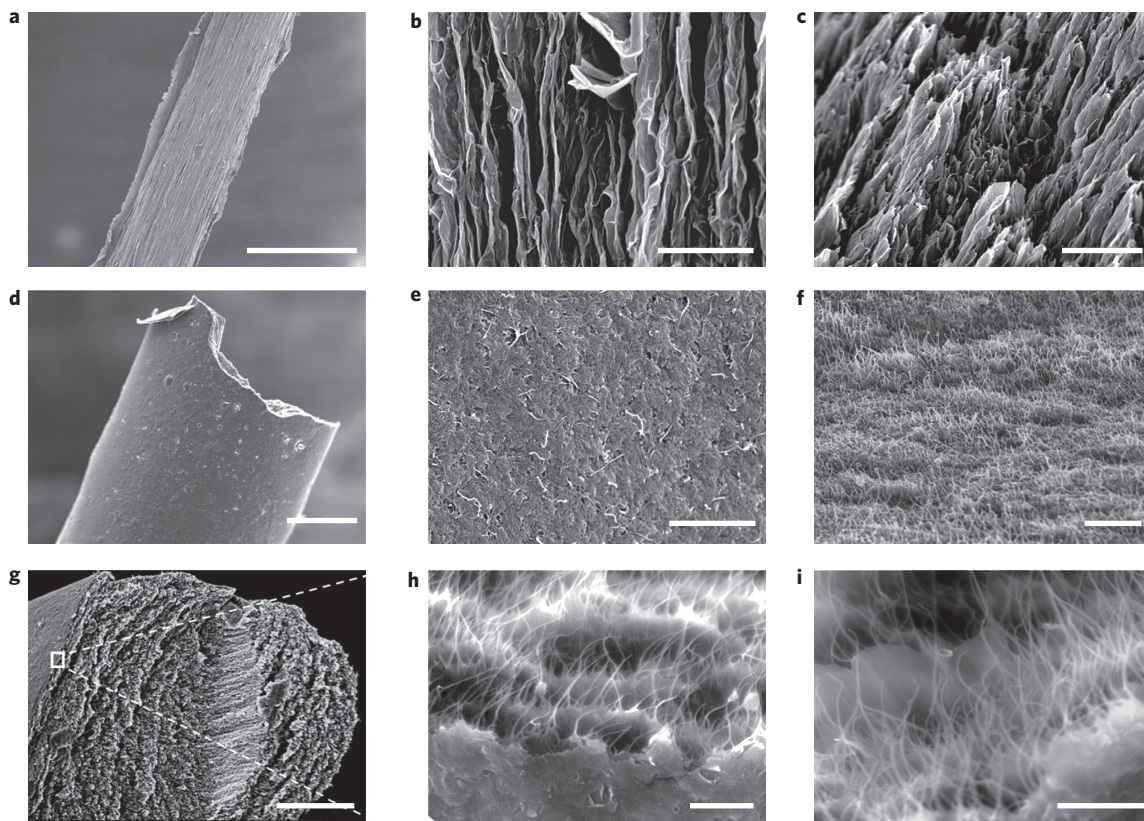


Figure 2 | Microstructures of the carbon hybrid microfibres. **a-f**, SEM images of the full view, outer surface and fracture end area of the rGO fibre (**a-c**) and fibre-3 (**d-f**). **g-i**, SEM images of the cross-section of fibre-3. In **h**, the square area in **g** is highlighted. In **i**, SWNT bundles are shown attached to the edges and surfaces of rGO. Scale bars: 50 μm (**a**), 20 μm (**d**), 15 μm (**g**), 1 μm (**c,f**), 0.5 μm (**b,e,h**), 300 nm (**i**).

Table 1 | Physical and chemical properties of hybrid carbon microfibres.

Fibres	SWNT:GO mass ratio	Diameter in wet/dry (μm)	Tensile strength (MPa)	Density of dry fibre (g cm^{-3})	Surface area ($\text{m}^2 \text{g}^{-1}$)	N doping (at%)	Conductivity (S cm^{-1})
rGO fibre	0:1	262 \pm 5/40 \pm 2	197	0.29 \pm 0.02	24	3.1	12
Fibre-1	1:8	275 \pm 6/45 \pm 2	165	0.36 \pm 0.03	108	2.9	20
Fibre-2	1:4	283 \pm 6/51 \pm 3	123	0.47 \pm 0.03	204	2.9	47
Fibre-3	1:1	294 \pm 7/60 \pm 3	84	0.59 \pm 0.04	396	2.8	102

surface area are two prerequisites for SC electrodes to achieve high volumetric performance^{7,8}. It was noted that both the density and surface area of our fibres increased with increasing SWNT fraction (Table 1) due to the aforementioned unique multiscale hierarchical structure, as revealed by scanning electron microscopy (SEM).

SEM images (Fig. 2a–c) show that the rGO fibre has densely stacked rGO sheets that are aligned along its main axis as a result of capillary forces during the drying process. Such dense stacking of the rGO leads to low accessible surface areas³⁸. In contrast, the specific surface areas of the hybrid fibres increased from 24 $\text{m}^2 \text{g}^{-1}$ to 396 $\text{m}^2 \text{g}^{-1}$ with increasing SWNT fraction from 0 to 50% (Table 1). The hybrid fibres have an interconnected porous structure (Fig. 2d–f). The aligned SWNTs interposed between the rGO layers not only reduce the stacking of the rGO, but also provide well-developed porosity in the hybrid fibre (Fig. 2g–i). As a result, fibre-3 has a specific surface area of 396 $\text{m}^2 \text{g}^{-1}$, much higher than those of carbon-based fibres reported so far, including rGO fibre (18 $\text{m}^2 \text{g}^{-1}$)³⁸, multiwalled CNT (MWCNT)-coated rGO fibre (89 $\text{m}^2 \text{g}^{-1}$)³⁸, dry-spun MWCNT fibre (100 $\text{m}^2 \text{g}^{-1}$)¹⁶, carbon microfibre (<10 $\text{m}^2 \text{g}^{-1}$)³⁹, CNT-coated carbon fibre (34.6 $\text{m}^2 \text{g}^{-1}$)³⁹ and wet-spun SWNT fibre (160 $\text{m}^2 \text{g}^{-1}$)⁴⁰. The nitrogen adsorption–desorption isotherm of fibre-3 (Supplementary

Fig. 5a) has a hysteresis loop, suggesting its mesoporous structure. The pore size distribution obtained from the Barrett–Joyner–Halenda method⁴¹ ranges from \sim 1.5 to 18 nm with a peak at \sim 5 nm (Supplementary Fig. 5b). Such a mesoporous structure is beneficial in providing a large accessible surface for fast ion transport. Therefore, it is the three-dimensional pillared vertically aligned SWNT/rGO assemblies confined within a one-dimensional fibre-like architecture that makes our fibres have both the high packing density and large ion-accessible surface area that are attractive for high-volumetric-performance SCs. For the hybrid fibres with a high SWNT fraction, SWNT alignment could be further enhanced by the inter-tube hydrogen-bonding interaction between the hydroxyl groups along the sidewalls of acid-treated SWNTs⁴². We noticed that when the fraction of SWNTs is low, a SWNT network could still form, albeit with a poor alignment along the fibre axis direction (Supplementary Fig. 6).

The fibres are susceptible to nitrogen doping during hydrothermal synthesis in the presence of EDA (Table 1), as confirmed by energy-dispersive X-ray spectroscopy, X-ray photoelectron spectroscopy, electron energy loss spectroscopy and Fourier-transform infrared spectroscopy (Supplementary Figs 7–11). It was found that EDA reacted with both the GO and acid-treated SWNTs via

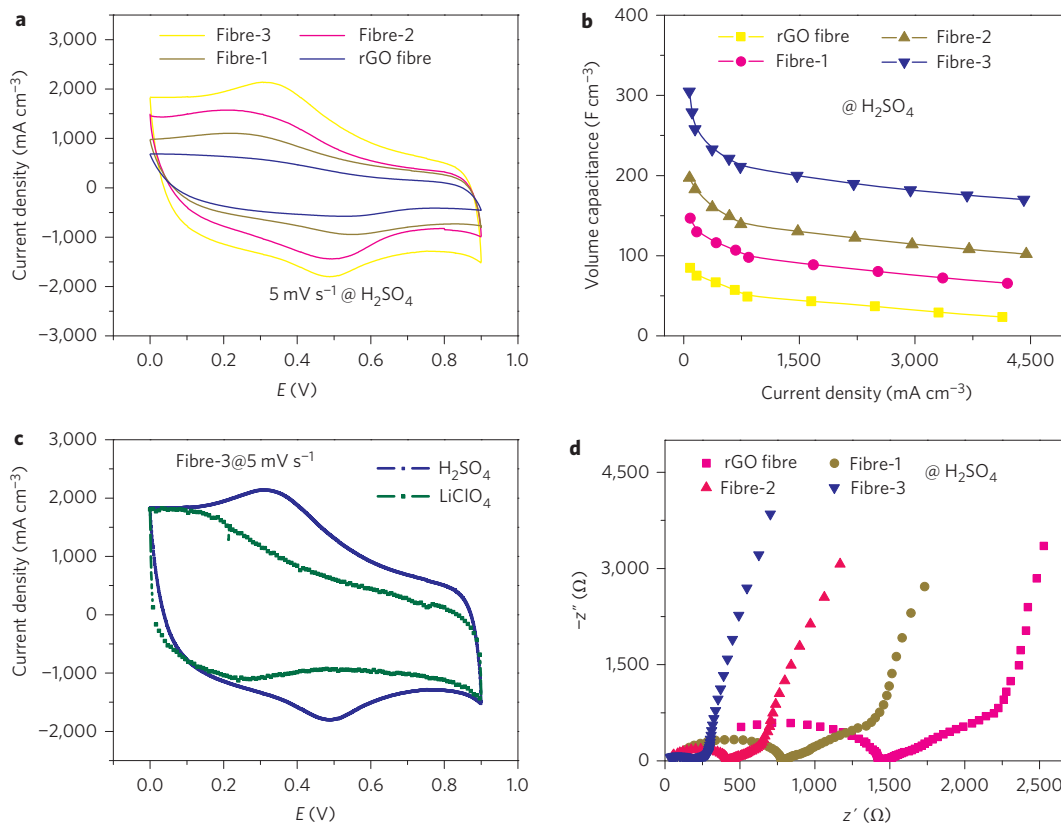


Figure 3 | Electrochemical performance of individual carbon hybrid microfibres in liquid electrolytes. **a,b**, Cyclic voltammetry curves (**a**) and specific volumetric capacitance (**b**) of the rGO fibre, fibre-1, fibre-2 and fibre-3 measured in a three-electrode configuration in 1 M H₂SO₄. **c**, Comparative cyclic voltammetry curves of fibre-3 at 5 mV s⁻¹ in 1 M LiClO₄ and H₂SO₄. **d**, Nyquist plots of the rGO fibre, fibre-1, fibre-2 and fibre-3 in 1 M H₂SO₄.

amide-bond linkage^{29,43}. Nitrogen was doped into the rGO framework as pyridinic and pyrrolic N (Supplementary Fig. 8e) during the hydrothermal process²⁹, but nitrogen doping to the acid-treated SWNTs was negligible (Supplementary Fig. 10), most probably because of the relatively low density of the surface carboxylic groups on the SWNTs. SWNT incorporation, coupled with nitrogen doping of rGO, significantly improved the electrical conductivity of the hybrid fibres (Supplementary Fig. 12). Hence, fibre-3 has a conductivity of 102 S cm⁻¹, which is about eight times higher than that of the rGO fibre (12 S cm⁻¹) and much better than those of previously reported rGO⁴⁴ and CNT fibres^{45,46}. Furthermore, our hybrid fibres showed negligible change in electrical conductivity over 1,000 bending cycles (Supplementary Fig. 12d), demonstrating their excellent structural stability.

Electrochemical characterization of fibre electrodes

We firstly tested the electrochemical performance of the as-synthesized fibres in a three-electrode cell in H₂SO₄. Their cyclic voltammetry (CV) curves at scan rates in the range 2–200 mV s⁻¹ and galvanostatic discharge curves at various current densities are shown in Fig. 3a and Supplementary Figs 13 and 14. The CV curves show reversible cathodic and anodic peaks at 0.3–0.5 V versus Ag/AgCl (Fig. 3a), indicating the presence of pseudocapacitance. The redox peaks disappear in neutral electrolyte (1 M LiClO₄) (Fig. 3c, Supplementary Fig. 15), suggesting that the pseudocapacitance was induced by oxygen-containing functional groups and/or nitrogen heteroatoms⁴⁶. The enhanced capacitive performance induced by nitrogen doping was further confirmed by comparative CV curves of the fibres with and without nitrogen doping (Supplementary Fig. 16). The specific volumetric capacitance (C_{sp}) of the fibres was calculated using their galvanostatic discharge

curves (Fig. 3b). It was found that fibre-3 has the highest specific volumetric capacitance of ~ 305 F cm⁻³ at ~ 73.5 mA cm⁻³ in 1 M H₂SO₄ in the three-electrode cell (or ~ 300 F cm⁻³ at ~ 26.7 mA cm⁻³ in polyvinyl alcohol (PVA)/H₃PO₄ electrolyte in a two-electrode cell, see below). To our knowledge, this is one of the highest values of specific volumetric capacitance among all reported porous carbon materials (Supplementary Table 1).

The observed large volumetric capacitances of the hybrid fibres can be attributed to the synergistic effect associated with their multi-scale hierarchical structures, in which rGO provides a large surface area for ion adsorption while the highly conductive aligned SWNT network reduces the rGO interlayer resistance and contact resistance with external circuits. Electrochemical impedance spectroscopic measurements show that the hybrid microfibres have much smaller equivalent series resistances than the rGO fibre (from the X-intercept of the Nyquist plot, Fig. 3d), and a nearly vertical line at the end of the semicircular region seen for fibre-3 (Fig. 3d). SWNT incorporation can reduce the stacking of the rGO to provide a large surface area with well-defined mesoporosity for efficient electrolyte penetration and ion adsorption, while increasing the bulk density of fibre-3 to ~ 0.6 g cm⁻³, which is twice that of common graphene materials (~ 0.3 g cm⁻³, $60\text{--}100$ F cm⁻³)⁴⁷. It was estimated that $\sim 40\%$ of the total capacitance of fibre-3 arises from the pseudocapacitance (Supplementary Fig. 17). The presence of oxygen-containing functional groups and nitrogen heteroatoms in the hybrid fibres increases their surface wettability (small contact angle of 53° , Supplementary Fig. 18), which enhances polar interactions with the electrolyte solution⁴³. This is not inconsistent with the smaller volumetric capacitance determined in the neutral electrolyte (Supplementary Fig. 15), in which the surface functional groups are not sufficiently polarized.

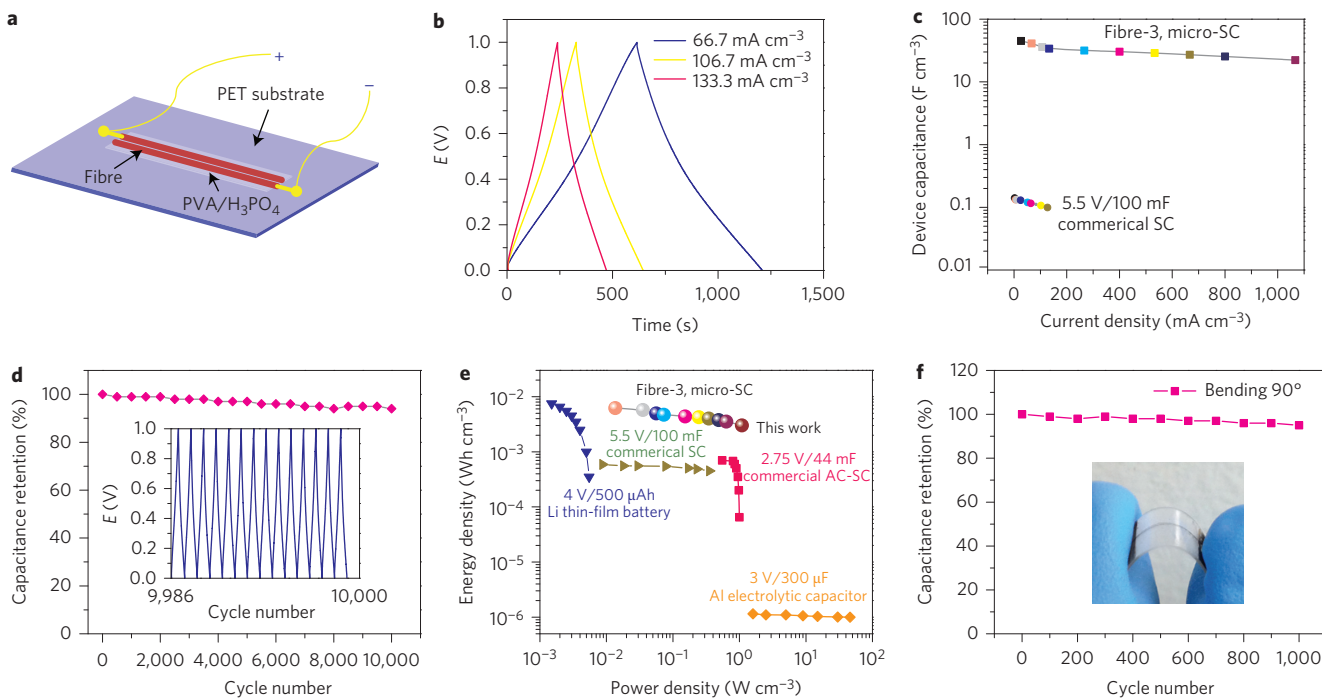


Figure 4 | Electrochemical performances of all-solid-state micro-SCs. **a**, Schematic of a micro-SC constructed using two fibre-3 electrodes on a polyester (PET) substrate. **b**, Galvanostatic charge/discharge curves at various current densities. **c**, Volumetric device capacitance at different current densities. Data obtained from a commercial activated carbon supercapacitor are also shown for comparison. **d**, Cycle life of the micro-SC. Inset: Galvanostatic charge/discharge curve after 10,000 cycles between 0 and 1 V at 250 mA cm⁻³. **e**, Energy and power densities of the micro-SC compared with commercially available state-of-the-art energy storage systems. Data for the lithium battery are from ref. 1 and data for the 2.75 V/44 mF activated carbon supercapacitor (AC-SC) is reproduced from ref. 3. **f**, Capacitance retention after 1,000 cycles up to 90° bending angle. Inset: Photograph of a bent micro-SC.

Testing of all-solid-state micro-SCs

We used fibre-3 (with the best capacitive performance measured in the three-electrode cell) as both active materials and current collectors to construct flexible micro-SCs (Fig. 4a). Typically, two parallel fibre-3 electrodes were mounted onto a flexible polyester (PET) substrate using PVA-H₃PO₄ electrolyte without binder, current collector, separator or any packaging material (see Supplementary Fig. 19 for a detailed description). The total volume of each micro-SC, including two fibres and the surrounding solid electrolytes, was estimated to be $\sim 7.5 \times 10^{-5}$ cm³. The CV curves of the micro-SC at various scanning rates (5–100 mV s⁻¹) have an almost rectangular shape within 0–1 V (Supplementary Fig. 20). Its galvanostatic charge/discharge curves (Fig. 4b) have a triangular shape with a coulombic efficiency of $\sim 98\%$, indicating excellent reversibility and good charge propagation between the two fibre electrodes. Figure 4c illustrates that the volumetric capacitance of the micro-SC ($C_{cell,V}$, normalized to the whole device volume) is ~ 45.0 F cm⁻³ at ~ 26.7 mA cm⁻³ and ~ 25.1 F cm⁻³ at ~ 800 mA cm⁻³, corresponding to area capacitances ($C_{cell,A}$) of ~ 116.3 mF cm⁻² and ~ 64.6 mF cm⁻², respectively, outperforming all previously reported carbon-based micro-SCs with capacitances in the range of 1–18 F cm⁻³ or 0.5–86 mF cm⁻² (Supplementary Tables 2 and 3). The specific volumetric capacitance of a single-fibre electrode (C_{sp}) in a two-electrode cell was calculated using galvanostatic discharge curves to be ~ 300 F cm⁻³ at ~ 26.7 mA cm⁻³ (Supplementary Table 2). Figure 4d shows that the micro-SC retains 93% of its initial capacitance after 10,000 charge/discharge cycles, demonstrating its impressive performance stability with a long cycle life, as is the case for other nitrogen-doped graphene materials⁴⁸.

The volumetric power/energy density of the whole SC is a more meaningful parameter for evaluating the energy storage performance of the microdevice than the gravimetric power/energy density based on active electrode materials⁸. The Ragone plots in

Fig. 4e compare the volumetric performance of our micro-SCs to those of commercially available energy-storage devices. Our micro-SC has a volumetric energy density ($E_{cell,V}$, normalized to the whole device volume) of ~ 6.3 mWh cm⁻³, which is about ten times higher than the energy densities of commercially available supercapacitors (2.75 V/44 mF and 5.5 V/100 mF, < 1 mWh cm⁻³)^{3,6} and even comparable to the 4 V/500 μAh thin-film lithium battery (0.3 – 10 mWh cm⁻³)¹. This energy density value is also higher than that of recently reported thin-film supercapacitors based on different two-dimensional materials, including laser-scribed graphene (~ 1.36 mWh cm⁻³ in ionic liquid)⁶ and transition-metal carbides and carbonitrides (Ti₃C₂ MXenes, ~ 1 mWh cm⁻³ in K₂SO₄)⁴⁷, and comparable to that of macroscale SCs based on graphene-derived three-dimensional porous carbon⁴⁹. The maximum volumetric power density ($P_{cell,V}$) for our micro-SCs is 1,085 mW cm⁻³, comparable to the commercially available supercapacitors and more than two orders of magnitude higher than that of lithium thin-film batteries^{1,6}. To our knowledge, the volumetric energy density in this work is the highest value among all carbon-based solid-state micro-SCs reported to date (Supplementary Tables 2 and 3).

The micro-SC was further subjected to mechanical bending tests. It shows negligible capacitance change ($< 0.05\%$) on bending to 90° (Supplementary Fig. 21). Furthermore, it retains more than 97% of its initial capacitance after bending 1,000 times at 90° (Fig. 4f), demonstrating the high flexibility and electrochemical stability desirable for flexible electronics.

Use of multiple micro-SCs to power nanosystems

To meet specific energy and power needs for practical applications, three micro-SCs were assembled both in series (Fig. 5a,b) and in parallel (Fig. 5c,d). Compared with a single micro-SC with an operating voltage of 1.0 V, the three micro-SCs connected in series

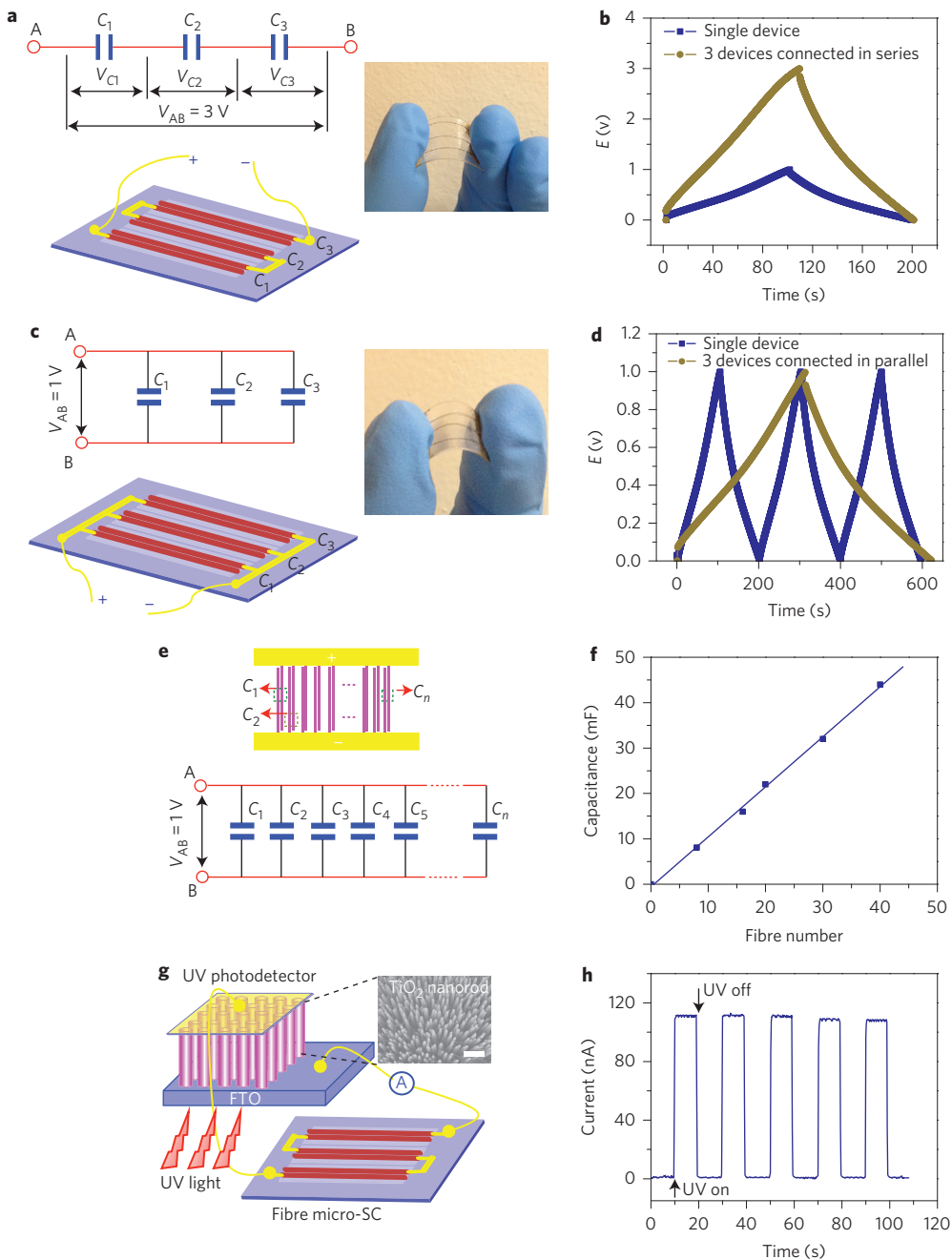


Figure 5 | Assembly of multiple microfibres in micro-SCs and their integration in a self-powered nanosystem. **a**, Schematic, equivalent circuit and photograph of the three micro-SCs connected in series. **b**, Galvanostatic charge/discharge curves of the device shown in **a**. **c**, Three micro-SCs connected in parallel. **d**, Galvanostatic charge/discharge curves of the device shown in **c**. **e**, Schematic and equivalent circuit for scalable integration of multiple fibres in micro-SCs in parallel. **f**, Relation between total device capacitance and number of fibres integrated. **g**, Schematic of a self-powered nanosystem. Inset: SEM image of an aligned TiO_2 nanorod array grown on an FTO substrate. Scale bar, $1\mu\text{m}$. **h**, Current response of the ultraviolet photodetector based on the TiO_2 nanorod array powered by the micro-SC (see **g**).

exhibited a 3 V charge/discharge voltage window (Supplementary Fig. 22) with similar discharge time (Fig. 5b). The output current of the parallel micro-SC assembly increased by a factor of three and its discharge time is three times that of a single micro-SC when operated at the same current density (Fig. 5d, Supplementary Fig. 23). Moreover, multiple micro-SCs were assembled in parallel by incorporating a different number of fibres (up to 40 fibres) (Fig. 5e,f). The overall capacitance of the assembled micro-SCs increased linearly with the number of fibres, showing good scalability.

To further demonstrate the potential applications of the fibre-based micro-SCs as efficient energy storage components for electronic and optoelectronic devices, we constructed a self-powered nanosystem, in which three fully charged micro-SCs were assembled in series to power an ultraviolet photodetector based on TiO_2 nanorod arrays grown on a fluorine-doped tin oxide (FTO) glass substrate⁵⁰ without any external bias voltage (Fig. 5g). Using the integrated micro-SCs as the external power source, the photodetector has a steady response to ultraviolet light irradiation ($\lambda = 254\text{ nm}$), as shown in Fig. 5h. Fully charged integrated

multiple micro-SCs can also be used to power a light-emitting diode, as shown in Supplementary Fig. 24.

Conclusions

Using a silica capillary column as a linear hydrothermal microreactor, we have developed a scalable method to continuously produce carbon microfibres with hierarchical structures comprising nitrogen-doped rGO and acid-oxidized SWNTs. Directed assembly of these two carbon components within the microfibre confinement in the presence of ethylenediamine led to the formation of three-dimensional pillared assemblies along the fibre length. The resultant hybrid fibre exhibits high packing density and large ion-accessible surface area, as is desirable for high-volumetric-performance micro-SCs. Our fibre has a conductivity of 102 S cm^{-1} and a specific surface area of $396 \text{ m}^2 \text{ g}^{-1}$. We have shown that the capacitor electrodes fabricated from these fibres have a specific volumetric capacity of 305 F cm^{-3} in H_2SO_4 (at 73.5 mA cm^{-3} , in a three-electrode cell) and 300 F cm^{-3} in PVA/ H_3PO_4 (at 26.7 mA cm^{-3} , in a two-electrode cell). An all-solid-state micro-SC made from two such parallel fibre electrodes on a flexible polymeric substrate, using PVA/ H_3PO_4 as the gelled electrolyte, without binder, current collector, separator or any other packaging material, exhibited a long cycle life (93% device capacitance retention over 10,000 cycles) and an ultrahigh volumetric energy density of $\sim 6.3 \text{ mWh cm}^{-3}$, about tenfold higher than those of state-of-the-art commercial supercapacitors and even comparable to the $4 \text{ V}/500 \mu\text{Ah}$ thin-film lithium battery. The micro-SC delivers a maximum power density of up to $1,085 \text{ mW cm}^{-3}$, a value comparable to that of typical commercially available supercapacitors and more than two orders higher than the power density of lithium thin-film batteries. Our micro-SCs can be integrated either in series or in parallel to meet the energy and power needs in various potential applications, including portable flexible optoelectronics, multifunctional textiles, sensors and energy devices, as exemplified in this study by powering a TiO_2 -based ultraviolet photodetector and a light-emitting diode. Our device could bridge the energy density gap between microbatteries and micro-SCs for miniaturized portable electronics. The synthetic methodology we have developed is scalable and the resultant hierarchically structured fibres could be regarded as a general architecture for designing functional hybrid microfibres.

Methods

Synthesis of carbon hybrid fibres. GO was prepared from natural graphite flakes by a modified Hummers' method, as previously described⁵¹. SWNTs (Carbon Solution, AP-SWNT, with diameters around 1.4 nm) were oxidized by nitric acid reflux for 4 h. The homogeneous acid-oxidized SWNT/GO aqueous dispersions at different SWNT/GO mass ratios of 1:8, 1:4 and 1:1 were prepared by adding a predetermined amount of functionalized SWNTs into 5 ml GO aqueous solution (8 mg ml^{-1}), followed by the addition of 5 μl EDA. The dispersion was injected into a flexible fused-silica capillary column (0.5 mm inner diameter; Biotaq, BT-G-530680) by a peristaltic pump (Shimadzu, LC-20AT). The capillary column was placed in a furnace with one end connected to the peristaltic pump and a nitrogen cylinder through a three-way valve, and the other end terminated by a one-way valve. Because of their flexibility and thermal stability, a long column (up to metres) can be easily packed into a small furnace. The capillary column served as a hydrothermal reactor, and was heated at 220°C for 6 h with both valves closed. After cooling to room temperature, the resultant wet fibre was pushed out by nitrogen flow into a water reservoir. Thereafter, the wet fibre was dried in air for 4 h.

Electrochemical characterization of individual fibres. A three-electrode cell, consisting of an Ag/AgCl (3 M KCl) electrode as the reference electrode, a platinum wire as the counter electrode and a single fibre as the working electrode in 1 M H_2SO_4 or LiClO_4 electrolyte, was used for capacitance measurements by a potentiostat (CHI 660D). The specific volumetric capacitance (C_{sp}) of the fibres in a three-electrode cell was calculated according to

$$C_{sp} = C_{electrode}/V_{fibre} \quad (1)$$

where $C_{electrode}$ is the measured capacitance in the three-electrode configuration and V_{fibre} is the volume of the fibre used as the working electrode. The fibre is considered

to be a cylinder to calculate its volume. $C_{electrode}$ was calculated from the galvanostatic discharge curves, using the equation

$$C_{electrode} = i/(dV/dt) \quad (2)$$

where i is the discharge current, and dV/dt is the slope of the discharge curve. Alternatively, $C_{electrode}$ was also calculated using the voltammetric charge integrated from CV curves according to the formula

$$C_{electrode} = \frac{Q}{2V} = \frac{1}{2Vv} \int_{V_-}^{V_+} i(V)dV \quad (3)$$

where Q is the total voltammetric charge obtained by integrating the positive and negative sweeps ($i(V)$ is the current) of a CV curve, v is the scan rate, and $V (V = V_+ - V_-)$ represents the scanned potential window of 0.9 V used in the three-electrode cell in this study.

Fabrication and characterization of all-solid-state micro-SCs. The polymeric gel electrolyte (PVA/ H_3PO_4) was prepared according to a previously reported method²⁰ (Supplementary Methods 2). Two dry fibres with the same length and from the same synthesis batch were immersed in the PVA/ H_3PO_4 electrolyte solution for 5 min. Thereafter, the electrolyte wetted fibres were placed on a PET film, in parallel, and their position was adjusted under an optical microscope (HI-Scope Advanced KH-3000, X700). Finally, the assembled device was dried under ambient conditions until the PVA/ H_3PO_4 gel solidified. The performance of the assembled micro-SCs was evaluated by CV and galvanostatic charge/discharge in a two-electrode configuration using the potentiostat (CHI 660D). Two commercial capacitors were also tested, including a supercapacitor (NEC Tokin, 5.5 V 0.1 F) and an aluminium electrolytic capacitor (Mouse Electronics, 75-TE1066-E3, 3 V, 300 μF). The capacitance of the supercapacitors (C_{cell}) in a two-electrode cell was calculated from their galvanostatic charge/discharge curves at different current densities using

$$C_{cell} = i/(dV/dt) \quad (4)$$

where i is the discharging current and dV/dt is the slope of the discharge curve. Alternatively, C_{cell} can be also calculated from CV curves using

$$C_{cell} = \frac{Q}{2V} = \frac{1}{2Vv} \int_{V_-}^{V_+} i(V)dV \quad (5)$$

where Q is the total voltammetric charge obtained by integration of the positive and negative sweeps ($i(V)$ is the current) in a CV curve, v is the scan rate, and $V (V = V_+ - V_-)$ represents the scanned potential window of 1 V.

The calculation methods of the specific volumetric capacitance at one electrode (C_{sp}) in a two-electrode cell are described in detail in Supplementary Methods 4.

The device areal and volumetric capacitances of the SCs were calculated according to the equations

$$C_{cell,A} = C_{cell}/A_{cell} \quad (6)$$

$$C_{cell,V} = C_{cell}/V_{cell} \quad (7)$$

where A_{cell} and V_{cell} refer to the device area and volume of the micro-SCs, respectively. The calculation of A_{cell} and V_{cell} is described in Supplementary Fig. 19.

The volumetric energy density of the SCs ($E_{cell,V}$) was obtained from the equation

$$E_{cell,V} = C_{cell,V} \Delta E^2 / (2 \times 3,600) \quad (8)$$

where ΔE is the operating voltage window in volts.

The volumetric power density of the SCs ($P_{cell,V}$) was calculated from the galvanostatic curves at different charge/discharge current densities using the equation

$$P_{cell,V} = E_{cell,V} \times 3,600/t_{discharge} \quad (9)$$

where $t_{discharge}$ is the discharge time.

Received 27 November 2013; accepted 8 April 2014;
published online 11 May 2014; corrected online 27 May 2014

References

- Pech, D. *et al.* Ultrahigh-power micrometre-sized supercapacitors based on onion-like carbon. *Nature Nanotech.* **5**, 651–654 (2010).
- Gao, W. *et al.* Direct laser writing of micro-supercapacitors on hydrated graphite oxide films. *Nature Nanotech.* **6**, 496–500 (2011).

3. El-Kady, M. F. & Kaner, R. B. Scalable fabrication of high-power graphene micro-supercapacitors for flexible and on-chip energy storage. *Nature Commun.* **4**, 1475 (2013).
4. Bae, J. *et al.* Fibre supercapacitors made of nanowire-fibre hybrid structures for wearable/flexible energy storage. *Angew. Chem. Int. Ed.* **50**, 1683–1687 (2011).
5. Chmiola, J., Largeot, C., Taberna, P. L., Simon, P. & Gogotsi, Y. Monolithic carbide-derived carbon films for micro-supercapacitors. *Science* **328**, 480–483 (2010).
6. El-Kady, M. F., Strong, V., Dubin, S. & Kaner, R. B. Laser scribing of high performance and flexible graphene-based electrochemical capacitors. *Science* **335**, 1326–1330 (2012).
7. Yang, X., Cheng, C., Wang, Y., Qiu, L. & Li, D. Liquid-mediated dense integration of graphene materials for compact capacitive energy storage. *Science* **341**, 534–537 (2013).
8. Gogotsi, Y. & Simon, P. True performance metrics in electrochemical energy storage. *Science* **334**, 917–918 (2011).
9. Nam, I. *et al.* Interdigitated supercapacitor chips are fabricated using pseudo-capacitive metal oxide electrodes. *Nanoscale* **4**, 7350–7353 (2012).
10. Sun, W. & Chen, X. Y. Fabrication and tests of a novel three dimensional microsupercapacitor. *Microelectron. Eng.* **86**, 1307–1310 (2009).
11. Wang, K. *et al.* An all-solid-state flexible micro-supercapacitor on a chip. *Adv. Energy Mater.* **1**, 1068–1072 (2011).
12. Liu, W., Feng, Y., Chen, J. & Xue, Q. Superior micro-supercapacitors based on graphene quantum dots. *Adv. Funct. Mater.* **23**, 4111–4122 (2013).
13. Beidaghi, M. & Wang, C. Micro-supercapacitors based on interdigital electrodes of reduced graphene oxide and carbon nanotube composites with ultrahigh power handling performance. *Adv. Funct. Mater.* **22**, 4501–4510 (2012).
14. Yang, P. *et al.* Hydrogenated ZnO core-shell nanocables for flexible supercapacitors and self-powered systems. *ACS Nano* **7**, 2617–2626 (2013).
15. Lee, V. T. *et al.* Coaxial fibre supercapacitor using all-carbon material electrodes. *ACS Nano* **7**, 5940–5947 (2013).
16. Chen, X. *et al.* Novel electric double-layer capacitor with a coaxial fibre structure. *Adv. Mater.* **25**, 6436–6441 (2013).
17. Ren, J., Bai, W., Guan, G., Zhang, Y. & Peng, H. Flexible and weaveable capacitor wire based on carbon nanocomposite fibre. *Adv. Mater.* **25**, 5965–5970 (2013).
18. Meng, Y., Zhao, Y., Hu, C., Cheng, H. & Hu, Y. All-graphene core-sheath microfibres for all-solid-state, stretchable fibriform supercapacitors and wearable electronic textiles. *Adv. Mater.* **25**, 2326–2331 (2013).
19. Ren, J. *et al.* Twisting carbon nanotube fibres for both wire-shaped micro-supercapacitor and micro-battery. *Adv. Mater.* **24**, 1155–1159 (2012).
20. Xiao, X. *et al.* Fibre-based all-solid-state flexible supercapacitors for self-powered systems. *ACS Nano* **6**, 9200–9206 (2012).
21. Tao, J. *et al.* Solid-state high performance flexible supercapacitors based on polypyrrole-MnO₂-carbon fibre hybrid structure. *Sci. Rep.* **3**, 2286 (2013).
22. Lee, J. A. *et al.* Ultrafast charge and discharge biskrolled yarn supercapacitors for textiles and microdevices. *Nature Commun.* **4**, 1970 (2013).
23. Zhao, Y. *et al.* A versatile, ultralight, nitrogen-doped graphene framework. *Angew. Chem. Int. Ed.* **51**, 11371–11375 (2012).
24. Yu, D. & Dai, L. Self-assembled graphene/carbon nanotube hybrid films for supercapacitors. *J. Phys. Chem. Lett.* **1**, 467–470 (2010).
25. Jha, N., Ramesh, P., Bekyarova, E., Itkis, M. E. & Haddon, R. C. High energy density supercapacitor based on a hybrid carbon nanotube-reduced graphite oxide architecture. *Adv. Energy Mater.* **2**, 438–444 (2012).
26. Zhu, Y. *et al.* A seamless three-dimensional carbon nanotube graphene hybrid material. *Nature Commun.* **3**, 1225 (2012).
27. Du, F. *et al.* Preparation of tunable 3D pillared carbon nanotube-graphene networks for high-performance capacitance. *Chem. Mater.* **23**, 4810–4816 (2011).
28. Lin, J. *et al.* 3-dimensional graphene carbon nanotube carpet-based microsupercapacitors with high electrochemical performance. *Nano Lett.* **13**, 72–78 (2013).
29. Chen, P. *et al.* Hydrothermal synthesis of macroscopic nitrogen-doped graphene hydrogels for ultrafast supercapacitor. *Nano Energy* **2**, 249–256 (2013).
30. Cote, L. J. *et al.* Graphene oxide as surfactant sheets. *Pure Appl. Chem.* **83**, 95–110 (2011).
31. Gong, K. P. *et al.* Nitrogen-doped carbon nanotube arrays with high electrocatalytic activity for oxygen reduction. *Science* **323**, 760–764 (2009).
32. Yu, D., Zhang, Q. & Dai, L. Highly efficient metal-free growth of nitrogen-doped single-walled carbon nanotubes on plasma-etched substrates for oxygen reduction. *J. Am. Chem. Soc.* **132**, 15127–15129 (2010).
33. Song, S. *et al.* Reversible self-assembly of terpyridine functionalized graphene oxide for energy conversion. *Angew. Chem. Int. Ed.* **53**, 1415–1419 (2013).
34. Li, Y., Li, Z. & Shen, P. Simultaneous formation of ultrahigh surface area and three-dimensional hierarchical porous graphene-like networks for fast and highly stable supercapacitors. *Adv. Mater.* **25**, 2474–2480 (2013).
35. Dong, Z. L. *et al.* Facile fabrication of light, flexible and multifunctional graphene fibres. *Adv. Mater.* **24**, 1856–1861 (2012).
36. Xu, Z. & Gao, C. Graphene chiral liquid crystals and macroscopic assembled fibres. *Nature. Commun.* **2**, 571 (2011).
37. Ericson, L. M. *et al.* Macroscopic, neat, single-walled carbon nanotube fibres. *Science* **305**, 1447–1450 (2004).
38. Cheng, H. *et al.* Textile electrodes woven by carbon nanotube/graphene hybrid fibres for flexible electrochemical capacitors. *Nanoscale* **5**, 3428–3434 (2013).
39. Zhao, X., Lu, X., Tze, W. T. Y. & Wang, P. A single carbon fibre microelectrode with branching carbon nanotubes for bioelectrochemical processes. *Biosens. Bioelectron.* **25**, 2343–2350 (2010).
40. Neimark, A. V., Ruetsch, S., Kornev, K. G. & Ravikovich, P. I. Hierarchical pore structure and wetting properties of single-wall carbon nanotube fibres. *Nano Lett.* **3**, 419–423 (2003).
41. Xu, Z., Zhang, Y., Li, P. & Gao, C. Strong, conductive, lightweight, neat graphene aerogel fibres with aligned pores. *ACS Nano* **6**, 7103–7113 (2011).
42. Pan, H. L. *et al.* Well-aligned carbon nanotubols from mechanochemical reaction. *Nano Lett.* **3**, 29–32 (2003).
43. Byon, H. R., Lee, S. W., Chen, S., Hammond, P. T. & Shao-Horn, Y. Thin films of carbon nanotubes and chemically reduced graphenes for electrochemical microcapacitors. *Carbon* **49**, 457–467 (2011).
44. Cong, H. P., Ren, X.-C., Wang, P. & Yu, S. H. Wet-spinning assembly of continuous, neat, and macroscopic graphene fibres. *Sci. Rep.* **2**, 613 (2012).
45. Lu, W., Zu, M., Byun, J. H., Kim, B. S. & Chou, T. W. State of the art of carbon nanotube fibres: opportunities and challenges. *Adv. Mater.* **24**, 1805–1833 (2012).
46. Gao, F., Viry, L., Maugey, M., Poulin, P. & Mano, N. Engineering hybrid nanotube wires for high-power biofuel cells. *Nature Commun.* **1**, 2 (2010).
47. Lukatskaya, M. R. *et al.* Cation intercalation and high volumetric capacitance of two-dimensional titanium carbide. *Science* **341**, 1502–1505 (2013).
48. Jeong, H. M. *et al.* Nitrogen-doped graphene for high-performance ultracapacitors and the importance of nitrogen-doped sites at basal planes. *Nano Lett.* **11**, 2472–2477 (2011).
49. Tao, Y. *et al.* Towards ultrahigh volumetric capacitance: graphene derived highly dense but porous carbons for supercapacitors. *Sci. Rep.* **3**, 2975 (2013).
50. Kumar, A., Madaria, A. R. & Zhou, C. W. Growth of aligned single-crystalline rutile TiO₂ nanowires on arbitrary substrates and their application in dye-sensitized solar cells. *J. Phys. Chem. C* **114**, 7787–7792 (2010).
51. Liu, S. B. *et al.* Antibacterial activity of graphite, graphite oxide, graphene oxide, and reduced graphene oxide: membrane and oxidative stress. *ACS Nano* **5**, 6971–6980 (2011).

Acknowledgements

This work was supported by the Ministry of Education, Singapore (MOE2011-T2-2-062 and 2013-T1-002-132), the Asian Office of Aerospace Research and Development of the US Air Force (FA23861314110) and the US Air Force Office of Scientific Research (FA9550-12-1-0037 and FA9550-12-1-0069). The authors thank B. Zhang, D. S. Su and L. Hu for TEM analysis.

Author contributions

D.Y., L.D. and Y.C. conceived and designed the experiments. D.Y. carried out fibre synthesis and supercapacitor fabrication and testing. D.Y., K.G., H.W., L.W., W.J. and Q.Z. performed material characterization. D.Y., L.D. and Y.C. analysed the data and co-wrote the paper. All authors discussed the results and commented on the manuscript.

Additional information

Supplementary information is available in the online version of the paper. Reprints and permissions information is available online at www.nature.com/reprints. Correspondence and requests for materials should be addressed to L.D. and Y.C.

Competing financial interests

The authors declare no competing financial interests.

CORRIGENDUM

Scalable synthesis of hierarchically structured carbon nanotube-graphene fibres for capacitive energy storage

Dingshan Yu, Kunli Goh, Hong Wang, Li Wei, Wenchao Jiang, Qiang Zhang, Liming Dai and Yuan Chen

Nature Nanotechnology <http://dx.doi.org/10.1038/nnano.2014.93> (2014); published online 11 May 2014; corrected online 27 May 2014.

In the version of this Article originally published online, the author list in ref. 40 was incorrect. This error has now been corrected in all versions of the Article.